Study of the mechanical, electrical and morphological properties of PU/MWCNT composites obtained by two different processing routes

Borja Fernández-d'Arlas, Umar Khan, Lorena Rueda, Loli Martin, Jose A. Ramos, Jonathan N. Coleman, Maria L. González, Angel Valea, Iñaki Mondragon, Maria A. Corcuera, Arantxa Eceiza

PII: S0266-3538(11)00399-X
DOI: 10.1016/j.compscitech.2011.11.007
Reference: CSTE 5100

To appear in: *Composites Science and Technology*

Received Date: 11 November 2010
Revised Date: 4 November 2011
Accepted Date: 6 November 2011

Please cite this article as: Fernández-d'Arlas, B., Khan, U., Rueda, L., Martin, L., Ramos, J.A., Coleman, J.N., González, M.L., Valea, A., Mondragon, I., Corcuera, M.A., Eceiza, A., Study of the mechanical, electrical and morphological properties of PU/MWCNT composites obtained by two different processing routes, *Composites Science and Technology* (2011), doi: 10.1016/j.compscitech.2011.11.007

Study of the mechanical, electrical and morphological properties of PU/MWCNT composites obtained by two different processing routes

Borja Fernández-d'Arlas[1], Umar Khan[2], Lorena Rueda[1], Loli Martin[1], Jose A. Ramos[1], Jonathan N. Coleman[2], Maria L. González[3], Angel Valea[3], Iñaki Mondragon[1], Maria A. Corcuera[1], Arantxa Eceiza[1*]

[1] *"Materials+Technologies" Group, Polytechnic School. University of the Basque Country (UPV/EHU), Pza. Europa 1, 20018 Donostia-San Sebastián, Spain*

[2] *"Chemical-Physics of 1-D Nanostructures" Group, School of Physics. Trinity College of Dublin, Dublin 2, Ireland*

[3] *Escuela Universitaria de Ingeniería Técnica de Bilbao. University of the Basque Country (UPV/EHU), Pza. La Casilla 3, 48012 Bilbao, Spain*

* Corresponding author

tel.: (0034)-943-017185

e-mail: arantxa.eceiza@ehu.es

Abstract

A comparative study of the influence of processing route on polyurethanes (PU)/ Multiwalled carbon nanotube (MWCNT) composites mechanical and electrical properties and also morphology was undergone employing two differentiated processing methods, solvent casting and buckypaper infiltration, for producing PU composites with low, medium and high mass fractions of acid treated MWCNT, and with no covalent linkages between the matrix and the nanotubes. As for example, with a MWCNT mass fraction of ~ 18 wt% the second method produced stiffer (270 MPa), lighter (948 kg m^{-3}) and more electrically conductive (1.8 S cm^{-1}) composite while the first one gave softer (111 MPa) and more ductile (141%) materials. These properties differences are related to the different PU/MWCNT dispositions obtained through each synthesis route. Nanotubes percolating concentration is found to be crucial on composite properties evolution and a preferential interaction of MWCNT with PU hard segments is observed for solvent cast composites.

Key words:

A. Carbon Nanotubes

A. Polymer-matrix composites (PMCs)

B. Mechanical properties

E. Casting

E. Buckypaper infiltration

1.Introduction

Smartly engineering carbon nanotubes structures may lead to a new range of multifunctional smart composite materials [1,2] due to the outstanding mechanical [3] and electrical properties [4,5] of nanotubes. However preparation of advanced composite materials based on carbon nanotubes is still an issue due to the difficulty to benefit from their exceptional properties at the macroscale. Therefore understanding composites processing influence on final materials properties must be considered important in order to fix optimal processing methodologies that develop materials with the appropriate properties for the different applications.

Solvent casting approach has been regarded by many researches as a fairly effective way of dispersing CNT into polymer matrices [6,7]. On the other hand buckypapers (BPs) consisting on entangled CNT networks having a highly porous mesh structure, which along the pure carbon nature of the CNT, make them low density materials with moderate rigidity and fairly high strength [8,9] with the potential to create high CNT content light-weight and strong materials [10,11] with additional electrical properties [12-15]. Mechanical properties of BPs have been previously studied by other research groups relating them with their porosity, nanotube type, and nanotube-nanotube junctions density [16]. Elastic modulus E, strain at break, ε_{max}, and the strength, σ_c, trend to increase with the junctions' density. The drawback of this phenomenon is that density also increases with the number of junctions, so that if light-weight and strong materials are pursued at once, a compromise between number of junctions and materials final density is required when fabricating 100 wt% CNT sheet or BP. Another approach to improve CNT sheets mechanical properties is by intercalating polymers which bind the whole CNT network together acting as adhesives [11,17,18] and getting improved mechanical properties.

Combination of CNT with polyurethanes (PU), which can be considered as very tuneable block copolymers consisting on nanophase separated hard segments, HS, and soft segments, SS, may lead to complex ternary composite systems with synergetic effects on final composites mechanical properties. To elucidate the effects of CNT concentration and composite processing, in this work a set of thermoplastic polyurethane/multiwalled carbon nanotubes (PU/MWCNT) was prepared by the solvent casting approach and compared with another set prepared by the BP polymer infiltration method. Although conceptually *in-situ* polymerised composites might give good mechanical properties, which also has been reported in some experimental works [19], difficulty of attaining a controlled polymer molecular weight and controlled polyurethane morphology [20] led to the interest of a fundamental study of the effects of well characterised PU interaction with nanotubes. In comparison to *in-situ* polymerised composites, solvent cast or infiltrated BP should also retain its thermoplasticity and solubility capability because of the absence of covalent bonds between the nanotubes and the PU matrix, while at the same time the methods allow to easily incorporate high fractions of MWCNT. Mechanical and electrical properties of the prepared materials are modelled and related to their nanostructure.

2. Experimental

2.1. Chemicals and materials

2.1.1. Polyurethane matrix

Polyurethane (PU) matrix was synthesised in our laboratory by the two shot polymerisation approach [21]. It consists on 10 wt% hard segment (with a solubility parameter of $\delta = 23.0$ $J^{1/2}$ $cm^{-3/2}$) formed by 1,6-hexamethylene diisocyanate (HDI) (Bayer, Desmour H) and 1,4-butanediol (BD) (Aldrich, 99% purity). Soft segments ($\delta =$

20.9 $J^{1/2}$ $cm^{-3/2}$) consisted on a polydiol, formed by polycaprolactone and polycarbonate blocks (Ravecarb 111, Polimeri Europa). This copolymer has a glass transition temperature of -80 ºC, a melting temperature peak at 5 ºC and an average molecular weigh of 2,020 g mol^{-1}, as measured by chemical titration following ASTM-D 4274-88 standard [22] for measuring the hydroxyl number. The polycaprolactone and polycarbonate blocks average polymerization degrees resulted to be 4 and 6, respectively, as calculated by combination of hydrogen nuclear magnetic resonance (^{1}H-NMR) analysis together with the obtained value of molecular weight.

2.1.2. Carbon nanotubes

Multiwalled carbon nanotubes (MWCNT, Nanocyl 3100, Belgium) were always purified with a 2 h strong acid treatment, consisting on a mixture of nitric and sulphuric acids in a HNO_3:H_2SO_4 ratio of 1:3, in a sonic bath (Selecta, ULTRASONS-H, 200W), followed by filtration using a polytetrafluoroethylene (PTFE) membrane with an average pore size of 0.2 μm (ALBET-PT-020-47-BL) after which water was rinsed through to wash up to neutral pH. The purification process was undergone in order to remove remaining catalyst particles but also to introduce functional carboxylic groups onto the nanotubes surface, so that they could improve their solubility in polar solvents such as water due to increased electrostatic repulsion between tubes and a better interaction with the solvent molecules. The ratio of introduced carboxylic groups was studied by thermogravimetric analysis as well as by a chemical backward titration [23]. Both techniques gave an acid group functionality of the same order with an average value of $1.4 \pm 0.5 \times 10^{-3}$ mol g^{-1} nanotube [24].

2.1.3. Solvent cast composites

Solvent cast PU/MWCNT composites were prepared using a mixture of dimethylformamide (DMF, boiling point: 165 ºC, δ = 24.7 $J^{1/2}$ $cm^{-3/2}$) and terahydrofuran (THF, boiling point 66 ºC, δ = 18.6 $J^{1/2}$ $cm^{-3/2}$) in a ratio 1:1, as solvent. This system was chosen so because amide solvents are found to be good carbon nanotube dispersants [25], while the THF has a low boiling point which allows an easier evaporation of the solvent from the cast composites. Firstly the required amount of acid treated nanotubes were suspended in 6 mL of the solvents mixture and sonicated under a high energy sonication tip (Bioblock Scientific, Vibra Cell 75043; 750 W) operated with an amplitude of 20% for 10 min. Afterwards the right amount of polymer was pipetted (between 4.5 and 6 mL, for high and low CNT content, respectively) from a polymer solution in the same solvents mixture, with a concentration of 50 mg mL^{-1}, to produce a total composite film weight of 300 mg. Then the PU/MWCNT/solvent mixture was sonicated again under the same conditions as mentioned above, after what the mixture was again sonicated in a low energy sonic bath for 2 h. The solutions were then drop cast into PTFE moulds of 4 cm x 4 cm x 1 cm and the solvent was evaporated under controlled temperature and vacuum conditions. The evaporation cycle was: 24 h at room temperature and 700 ± 40 mbar, 24 h at 60 ºC and 700 ± 40 mbar, and finally 24 h at 60 ºC and 200 ± 20 mbar.

2.1.4. Infiltrated buckypapers composites

The preparation of the buckypapers begun with the dispersion of 30 mg acid treated MWCNT into 250 mL DMF, using firstly a 30 min treatment in a low power sonic bath followed by 10 min treatment of high energy tip sonication. Then the MWCNT solutions were filtered through PTFE filter membranes with an average pore diameter of 0.2 μm and under a controlled vacuum pressure of 200 ± 20 mbar, in order to always

follow a determinate scheme and to attain the same degree of nanotubes entanglements in each buckypaper, before polymer infiltration.

Vacuum control was managed by connecting the vacuum oven or the filtration set-up to a vacuum pump provided with a vacuum control system (Vacuubrand, PC620NT series) with solvent recovery system. Therefore solvents were recovered and disposed accordingly.

High MWCNT loading composites were prepared by infiltration of different THF polymer concentrated solutions and quantities, always with a controlled pressure of 200 ± 20 mbar. Infiltration times were shorter for diluted solutions and smaller solution quantities. Typically 50 mL of 1 mg mL^{-1} solution were infiltrated in about 12 h, while 50 mL of 2 mg mL^{-1} needed around 24 h, and 100 mL of a 1 mg mL^{-1} solution required around 20 h to infiltrate. When around 12 h of infiltration time was achieved, infiltrating pressure was reduced in order to speed up the process down to 50 ± 10 mbar. Uniform composites films, with polymer apparently coating evenly the nanotubes, were obtained and peeled out of the filter membranes.

2.2. Characterisation

Final nanotube volume fraction into the composites, ϕ, was related to the nanotubes weight fraction, X_{MWCNT}, polymer density, $\rho_{Polymer}$, and nanotubes density, ρ_{MWCNT}, using the following Eq. [26]:

$$\phi = \frac{X_{MWCNT}}{X_{MWCNT} + \left(\rho_{MWCNT} / \rho_{Polymer}\right) - \left(\rho_{MWCNT} / \rho_{Polymer}\right) X_{MWCNT}}$$

The films density was calculated by measuring precisely materials dimensions with a calliper (Mitutoyo, DIGIMATIC CD-15CP) and a low-torque digital micrometer (Mitutoyo) of pieces of about 7 mm x 0.15 mm x 2.5 mm and by weighting them on a

thermo-gravimetrical analysis balance (Mettler Toledo, TGA/SDTA 851) with precision down to ± 0.001 mg. Typical weight values ranged between 0.5 and 4 mg.

Porosity, *P*, was calculated using the previously measured films density introduced into the following Eq. [27]:

$$P = 1 - \rho_{film}\left[\frac{X_{MWCNT}}{\rho_{MWCNT}} + \frac{(1 - X_{MWCNT})}{\rho_{Polymer}}\right]$$

where ρ_{film} corresponds to the densities of composite films. Nanotubes density [26] was taken to be 1,750 kg m^{-3}, and the density of the polymer, was measured as 1,100 kg m^{-3}. X_{MWCNT} is the nanotubes weight fraction into the composite. Density and porosity measurements results for the prepared buckypapers are gathered in Table 1. As expected, porosity was reduced due to polymer infiltration, what made increase the composite density to that of the polyurethane at around 6 wt% of nanotube loading. On the other hand, composites cast after solvent mixing did not present significance changes in density being it always similar to that of the neat polymer (~1,100 kg m^{-3}). This result also confirmed that density changes in buckypaperss were solely due to porosity changes.

Atomic force microscope (AFM, Nanoscope IIIa) was operated in the tapping mode, provided with tips of average radio of 10 nm and applying moderate forces (typically amplitude set points between 0.8 and 2 V and drive amplitudes of 50 to 500 mV). Scan rates were in the range of 0.8-1.2 Hz. Statistical analysis was performed for measuring nanotubes length and diameter in a number of images, and buckypaper topography was studied over recorded images. Nanotubes diameters were measured over topographic images by height steps analysis. Nanotubes lengths were measured using the AnalySIS-docu software for microscope imaging and image analysis. Buckypapers roughness was

studied by scanning the AFM probe over the sheet surface with similar conditions as above.

Scanning electron microscopy (SEM) analysis was performed using a JEOL JSM-7000F, with an accelerating voltage of 20 kV and a distance of 9.0 ± 0.5 mm. Buckypapers and their infiltrated composites were not coated with metal layer because of their high conductivity. Solvent cast composites with a MWCNT content lower than 20 wt%, were coated with a thin gold layer of about 5-10 nm thickness with a Bal-Tec SCD-004 sputtering equipment.

Tensile tests were performed with a constant crosshead speed of 100 mm min^{-1} for solvent cast composites and low MWCNT volume fraction infiltrated buckypapers, and with a strain rate of 1 mm min^{-1} for all buckypapers, with an initial crosshead distance of 8.5 ± 0.5 mm. Samples sizes were in the range of 80-140 μm in thickness and 2.5 mm in width. The equipment used (MTS insight 10) was provided with pneumatic grips (Advantage Pneumatic Grips) and with a load cell of 250 N. The results were averaged from a minimum of 3 specimens.

Dynamic mechanical thermal analysis (DMTA) was performed in the film extension mode using a TA-Q-800 analyser, with samples geometry similar to those employed in tensile tests. The crosshead distance was 12.5 ± 0.6 mm. The operation frequency was 1 Hz, the amplitude 25 μm, and samples were scanned from -100 ºC to 100 ºC with a heating rate of 3 ºC min^{-1}.

Electrical DC measurements were carried out using a two probe current intensity voltage scan from 0 to 5 V employing a semiconductor analyser (Keithley 4200-SCS). Resistance was calculated from the slope of current intensity versus voltage (I-V) curves and averaged from three measurements. Distances between silver paint printed electrodes and specimens width was measured with a digital calliper while thickness

was measured using a low-torque digital micrometer in order to normalise resistance values into conductivity (S cm^{-1}) values.

Fourier transformed infrared spectroscopy (FT-IR, Nicolet-Nexus) measurements were recorded at room temperature by the attenuated total reflectance spectroscopy method (ATR, Golden Gate, Specac) employing a resolution of 2 cm^{-1} and 24 scans.

Differential scanning calorimetry (DSC) analysis of solvent cast composites was performed in a Mettler Toledo 822e equipment with scanning rates of 10 ºC min^{-1} from -60 ºC to 200 ºC using nitrogen as purge gas and an electric intracooler as cooling source. Heat flow was normalised to polyurethane weight fraction into composites.

3. Results and Discussion

3.1 Materials synthesis and physical properties

The MWCNT underwent an acid treatment prior to be utilised in composites preparation. In this way purification and introduction of carboxylic functionalities were pursued. Diameter, *D*, and length, *l* averages of the MWCNT decreased from 14 ± 6 nm to 12 ± 5 nm and from 1,639 ± 1,331 nm to 740 ± 519 nm respectively, with the acid treatment, as analysed by atomic force microscopy (AFM). Length distributions of pristine and acid treated nanotubes are gathered in Fig. 1a,b. This might be related to the destruction of part of the outer MWCNT walls, along with a decrease in length caused by cutting and shortening their ends. In this work only purified/functionalised carbon nanotubes were used.

Structure of an obtained pristine 100 wt% MWCNT buckypaper sheet prepared by a MWCNT dispersion filtration (see methods), as analysed by means of AFM and scanning electron microscopy (SEM) is gathered in Fig. 1c,d. Average roughness was

studied by 3D topographic analysis of Fig. 1c, while sheet porosity was better observed in the SEM image, Fig. 1d.

When preparing polyurethane infiltrated buckypaper composites, as it is presented in Table 1, for a PU concentration of 1 mg mL^{-1}, increasing the amount of infiltrating solution did not increase significantly the amount of adsorbed polyurethane into the final composite, and therefore the final MWCNT volume fraction (ϕ) was nearly constant. This fact could be related to adsorption/desorption equilibrium phenomena of PU into the MWCNT network at that particular PU concentration. Increasing PU concentration in the infiltrating solution resulted to be a much more effective method to control PU/MWCNT ratio in the final composite. Infiltration of 50 mL of a 10 mg mL^{-1} PU solution led to a material with density similar to that of neat polyurethane, what suggested a fully saturation of buckypapers pores with PU.

3.2 Mechanical and electrical properties. Percolation threshold.

Fig. 2 presents the tensile curves of some of the materials prepared. The neat PU has high modulus/hard segment content ratio. With just 10 wt% of hard segment content, its elastic modulus, E_m, was 6.5 ± 0.6 MPa. There are many examples in literature [28] in which such a modulus value was just obtained using about 30 wt% of aromatic 4,4´-diphenylmethane diisocyanate (MDI) and butanediol (BD) as hard segment constituents, and using a polyol of about the same molecular weigh as that used as soft segment in this work. This fact must be related to the higher cristallinity of the 1,6-hexamethylene diisocyanate (HDI) based hard segments of the polyurethane employed in this work, in comparison to those based on MDI [21]. An advantage of using this high crystalline polyurethane with low hard segment contents is that while providing fairly good modulus it retains the benefits of a highly ductile material.

Sequentially increasing nanofiller addition to a hosting matrix leads to a situation in which for a given concentration the filler forms a continuous percolated network. Above this particular concentration dramatic variation in some properties is expected due to the formation of two co-continuous phases which affect in different ways to the final composite properties. The critical MWCNT percolation volume fraction, ϕ_p, was detected graphically from the sharp variation in properties at ϕ_p [29]. Normalised elastic modulus, E_c/E_m, being E_c the composite elastic modulus, relative composite strength σ_c/σ_m, being σ_c and σ_m the composite and matrix strengths respectively, electrical conductivity, σ_{DC}, data and ductility evolution with concentration showed a spike point at ϕ_p, as shown in Fig. 3a-d. This bending point, upon which the increase of properties was sharper, occurred around ϕ = 0.025 (4 wt%) as detected in Fig. 3b-d, but the decrease in ductility begun at lower concentrations as seen in Fig. 3a. These curves presented three typical regions. (I) Region in which nanotubes addition did not produce notable properties variation due to an ineffective load and electrical transfer to the polyurethane matrix; (II) Region where percolation takes part and two dimensional network formation develops and (III) Formation of a three dimensional nanotube entangled network.

For a similar order of MWCNT concentration composites prepared by the infiltration method (Fig.3b, triangles) presented higher electrical conductivities than those based on the solvent casting approach (Fig.3b, squares), probably due to a more direct contact between nanotubes in the network junction points. The lower percolation threshold observed by DC conductivity could be related to a tunnelling effect of electricity between different nanotubes through nanotubes-polymeric interfaces. In general the high percolation threshold values obtained (ϕ_p ~ 0.025, 4 wt%) as compared to other

systems found in literature [30] ($\phi_p \sim 0.005$) can be related with the low nanotubes aspect ratios.

Addition of MWCNT to PU by the solvent casting approach led in all cases to a reduction in ε_{max} of materials, being the reduction sharper up to ϕ_p, while beyond this concentration ε_{max} decrease was not so important. This fact can be related to a more restricted mobility of soft segments [31]. As an example, addition of 12 wt% MWCNT, what corresponds to a volume fraction of 0.08, decreases ε_{max} from 2,380 ± 135% to 340 ± 50%. Despite the extensibility reduction of this material, it can still be considered as ductile. In returns σ_c and E_c increased with ϕ as shown in Fig. 3c,d.

3.3. Mechanical properties modelling

The strength was increased from 7.0 ± 0.4 MPa to 26.2 ± 6.1 MPa for solvent cast composites with 20 wt% MWCNT (ϕ = 0.13), this providing evidence of stress transfer to MWCNT, quantified by the interfacial shear strength, τ_c, between the PU matrix and MWCNT. Eq. (1), known as Bowyer-Bader model [32], describes reinforcement by shear transfer between matrix and small fibres:

$$\sigma_c = (\eta_0 \eta_l \sigma_f - \sigma_m)\phi + \sigma_m \quad (1)$$

where σ_c, σ_f and σ_m stand for the composite, fibre and matrix strengths, respectively. The factors η_o and η_l are the orientation and length efficiency factors, respectively. The orientation factor takes values of η_o = 1 for aligned fibres, η_o = 3/8 for fibres oriented in plane and η_o = 1/5 for randomly oriented fibres [33]. When applied to elastic modulus Eq. (1) turns into:

$$E_c = (\eta_0 \eta_l E_f - E_m)\phi + E_m \quad (2)$$

For the present analysis σ_f and E_f were taken to be σ_f = 50 GPa [34], and E_f = 500 GPa [35]. When the fibre length is much smaller that the critical length, l_c, required to fully transfer the fibre strength to the composite the length efficiency factor, η_l, becomes $l/2l_c$ [32]. Considering η_o = 1 at fracture (i.e: stress induced fibre orientation) and using the so called Kelly-Thysson relation [36], $l_c/D = \sigma_f/2\tau_c$, Eq. (1) turns into $\sigma_c = (\tau_c l/D - \sigma_m)\phi + \sigma_m$, from where τ_c can be calculated from the slope of σ_c vs. ϕ. The τ_c calculated in such a way and using the l/D average ratio obtained by AFM, was of 2.7 MPa. This value lays within the interval of those calculated (in this manner) with σ_c vs ϕ data reported in the literature, which range between 0.5 MPa for solvent cast PU/MWCNT composites systems [37], to 14 MPa for aligned extruded PU/CNT fibres [38]. Using Kelly-Thysson relation, our τ_c would require a critical fibre aspect ratio, $(l/D)_c$ = 9,366, or taking the value of D = 12 nm, as obtained by AFM, a l_c of 112 μm. Having our nanotubes lengths in the range of 740 ± 519 nm, far below from l_c, we can consider being in the pull-out regime [39], as described by Eq. (1). It can be calculated that to make a l_c = 1,500 nm fibre (approximately that of common commercial carbon nanotubes) transfer its full strength at fracture, a $\tau_c \approx 233$ MPa would be required, what is still much higher than values reported to date for PU elastomers reinforced with CNT. The pure MWCNT buckypaper (i.e: without polymer infiltration, ϕ = 1) presented ε_{max} = 2.9 ± 0.1%, σ_c = 4.4 ± 0.2 MPa, and E_c = 202 ± 10 MPa. As seen in Fig. 2, PU infiltration favoured buckypaper ε_{max} and σ_c. The σ_c improvement in buckypapers with PU infiltration can be related to an adhesive [11] like behaviour of the polymer between MWCNT improving stress transfer over the whole MWCNT network. In any case buckypapers composites σ_c was not higher than those of the solvent cast composites. This could be related to higher amount of weak MWCNT-MWCNT contacts in the case

of buckypapers (Fig.3), which slip altogether under a certain stress, phenomena which could be related to a yield point of the MWCNT network structure. The maximum σ_c (26.2 ± 6.1 MPa) was obtained with the solvent cast composite with 20 wt% MWCNT (ϕ = 0.13). The maximum E_c achieved (368 ± 71 MPa) was in the infiltrated buckypaper with 73 wt% MWCNT (ϕ = 0.62). The modulus enhancement, as expressed as $dE_c/d\phi$, for solvent cast composites was of 361 ± 41 MPa (slope of the fit to data in Fig. 4b). Composites prepared by the buckypaper infiltration approach led to a modulus enhancement of $dE_c/d\phi \approx$ 1,526 ± 150 MPa. This difference can be related to tighter nanotubes entanglements in the case of infiltrated buckypapers, which lead to stiffer materials due to a higher density of entanglements between nanotubes owed to the synthesis procedure in which nanotubes can be slowly intertwined forming a continuous network as the one shown in Fig. 1d. The lower strength observed can be explained by considering that the MWCNT network provides stiffness up to a certain stress upon which nanotubes slippage lead to a rapidly crack propagation due to stress concentration in the points close to where slippage occurred.

When applying Eq. (2) with η_o = 1 (aligned fibres), as considered for τ_c calculation in Eq. (1), and utilising l_c obtained from Eq. (1), the modulus was overestimated for solvent cast composites. Prediction of this model is drawn with a dashed line in Fig. 4b,c. On the other hand, when introducing η_o = 1/5 (for randomly oriented fibres) the modulus prediction was excellent for composites with a MWCNT concentration of up to 8 wt% ($\phi \sim$ 0.05) and also high MWCNT content infiltrated buckypapers. The underestimation of the model of composites with higher concentrations could be due to the lack of consideration of MWCNT-MWCNT entanglements into the model. This model is drawn with a dotted line in Fig. 4b,c. The good modulus prediction for low concentrations by Eq. (2) when considering η_o = 1/5, suggests that nanotubes were

oriented during the tensile tests, being initially randomly orientated. This models fitted composites elastic modulus for composites with MWCNT concentrations below ϕ_p, where polymer-nanotube interactions prevail. The models doesn´t apply for concentration above ϕ_p because, upon this concentration nanotube-nanotube interaction becomes more important and were not considered into them. The Halpin-Tsai model [40] for randomly oriented fibres and the modulus prediction based on the general theory for percolative [41] systems resulted to also fit to the data very well, contrarily to the Guths rule [42] or to the rule of mixtures as modified by Cox [43] (Supplementary, Fig. S1).

3.4. Fracture surface analysis by SEM and AFM

An electron micrograph of the fracture surfaces of an infiltrated buckypaper with a MWCNT content of 18 wt% ($\phi = 0.12$), is shown in Fig. 5a, and exhibits a dented structure caused by the jointly strain and alignment of nanotubes with the polymer. This must also be related to the capability of the polymer to transfer stress to the whole MWCNT network, as was also observed in the mechanical tests. The nanotubes alignment along stress direction was also observed by AFM, as is shown in Fig. 5b,c for a 6 wt% MWCNT composite (and Supplementary, Fig. S2) before and after tensile testing respectively. The presence of many nanotubes aligned preferently in the stress direction suggests that, as also seen in infiltrated buckypapers composites, composites fracture is in the pull-out regime with alignment of the nanotubes along the stress direction, further confirming the above analysis based on mechanical approaches.

3.5. Network formation and dynamic-mechanical-thermal properties (DMA).

As can be seen in Fig. 6, loading the polyurethane with MWCNT slightly improved the storage modulus, $E'(T, \phi)$, below soft segment glass transition, $T_{g,Soft}$ (with a peak in tang δ at -40 ºC and a onset at around -60 ºC), while the value clearly improved above it, suggesting nanotubes are preferentially interacting with PU hard domains [44] as has been suggested to be the case in carboxylic functionalised nanotubes/polyurethane composites [31,45]. Further evidences of favoured interaction between PU hard segments and MWCNT were obtained by FT-IR and DSC, results that are gathered in Fig.7. As can bee seen in Fig.7a the increment of nanotube concentration made increase the ratio of hydrogen bonded species, adsorbing at lower frequencies in the carbonyl region. In the inset the ratio between hydrogen bonded urethane carbonyl stretching band peak absorbance, h_a, and the non-hydrogen bonded soft segments carbonyls stretching band peak absorbance, h_f is represented against nanotube concentration. The tendency observed suggests a formation of more PU-MWCNT hydrogen bonded structures, probably drawn by the more polar urethane groups. Calorimetric results presented in Fig 7b show that the introduction of nanotubes did prevent more the interactions between hard and soft segments (endotherm with peak around 50 ºC) in favour of hard segments-MWCNT interactions, appearing as an endotherm which increased with nanotubes concentration and shifted towards higher temperatures with increased nanotube content. Despite the preferential interaction of MWCNT with PU hard segments there is also an important stiffening of the soft phase and a reduction in its energy dissipating capability with nanotubes addition as observed in the evolution of tan δ with nanotubes concentration at around -40 ºC, seen in Fig.6. Percolated network formation must also account for the leapt in $E'(T, \phi)$ seen between composites containing 3 wt% and 8 wt% MWCNT, what agrees with the detected ϕ_p by tensile and electrical tests at $\phi = 0.025$ (4 wt%). Addition of nanotubes also led to a big increase in

critical heat distortion temperature (HDT), as indicated with an arrow in the upper part of Fig. 6. With 20 wt% MWCNT the thermo-mechanical stability was of over 100 ºC. Infiltrated buckypapers presented small modulus loss and lower temperature property dependence that the cast composites. Their $E'(T, \phi)$, as also detected by tensile measurements, were also superior in the whole range of temperatures.

Infiltration of polymers into buckypapers improved the bending capability of the network. This can also be related to an adhesive effect between nanotubes in the PU matrix which, with the aim of regaining their full free volume when the stress ceases, recovers the original spacing between them. On this regard if a low density bendable and strong material is pursued, a compromise in the PU/MWCNT ratio of the infiltrated buckypapers is required. As an example, an infiltrated buckypaper with final MWCNT loading of 73 wt% ($\phi = 0.62$) presented mechanical values of $E_c = 400 \pm 68$ MPa, $\sigma_c = 11.8 \pm 1.5$ MPa, and $\varepsilon_{max} = 7.8 \pm 4.6\%$, $\sigma_{DC} = 12$ S cm^{-1}, good bending resistance while keeping a density of 362 kg m^{-3}.

4. Conclusions

PU/MWCNT composites prepared by solvent casting and buckypaper infiltration with PU solutions approaches lead to significantly different materials which differ in density, stiffness and electrical conductivity, being infiltrated buckypapers lighter, stiffer and electrically more conductive, but less ductile than those produced by the solvent casting approach. Control of the PU/MWCNT ratio in the infiltrated buckypapers composites was more effective by varying PU concentration rather than by solution quantities.

The mechanical properties analysis together with the findings of nanotubes favoured alignments along the stress direction, shed light on the MWCNT modulus enhancement mechanism by nanotube re-orientation under stress, with a shear transfer reinforcing

mechanism at fracture. For mechanical properties modeling additional phenomena to nanofibre-polymer stress-transfer, like nanotubes flexibility, effect of outer shells stress transfer to concentric shells or nanotubes-nanotubes interactions could improve results over percolation threshold, but as we present a simple Bowyer-Bader model/approach can indeed model quite well elastic modulus of composites below percolation threshold concentration.

Acid treated MWCNT do preferably interact with PU hard segments. Further understanding on PU-MWCNT interactions and the ability to benefit from the known composites processing techniques might lead to a new range of elastomeric materials with improved strength and functionalities, interesting for different high performance materials applications.

References

[1] Ajayan PM, Stephan O, Colliex C, Trauth D. Aligned carbon nanotube arrays formed by cutting a polymer resin-nanotube composite. Science 1994; 265: 1212.

[2] Baughman RH, Zakhidov AA, de Heer WA. Carbon nanotubes-the route toward applications. Science 2002, 297: 787.

[3] Bower C, Rosen R, Jin L, Han J, Zhou O. Deformation of carbon nanotubes in nanotube-polymer composites. Applied Physics Letters 1999, 74: 3317.

[4] Liang W, Bockrath M, Bozovic D, Hafner JH, Tinkham M, Park H. Fabry-Perot interference in a nanotube electron waveguide. Nature 2001, 411: 665.

[5] Frank SP, Poncharal P, Wang ZL, de Heer WA. Carbon nanotube quantum resistors. Science 1998, 280: 1744.

[6] Jin L, Bower C, Zhou O. Alignment of carbon nanotubes in a polymer matrix by mechanical stretching. Applied Physics Letters 1998, 73: 1197.

[7] Shaffer MSP, Windle AH. Fabrication and characterization of carbon nanotube/poly(vinyl alcohol) composites. Advanced Materials 1999, 11: 937.

[8] Zhang M, Fang S, Zakhidov AA, Lee SB, Aliev AE, Williams CD, Atkinson KR, Baughman RH. Strong, transparent, multifunctional, carbon nanotube sheets. Science 2005, 309: 1215.

[9] Weber J, Holman T, Eindenshink T, Chen JJ. Using buckypaper as therapeutic aid in medical applications. U. S. Patent 2005/0074479 A1, 2005.

[10] Endo M, Muramatsu H, Hayashi T, Kim YA, Terrones M, Dresselhaus MS. Buckypaper of Coaxial Nanotubes. Nature 2005, 433: 476.

[11] Coleman JN, Blau WJ, Dalton AB, Muñoz E, Collins S, Kim BG, Razal J, Selvidge M, Vieiro G, Baughman RH. Improving the mechanical properties of single-walled carbon nanotube sheets by intercalation of polymeric adhesives. Applied Physics Letters 2003, 82: 1682.

[12] Hu L, Hecht DS, Grüner G. Percolation in transparent and conducting carbon nanotube networks. Nano Letters 2004, 4: 2513.

[13] Kaempgen M, Duesberg GS, Roth S. Transparent carbon nanotube coatings. Applied Surface Science. 2005, 252: 425.

[14] Zhou Y, Hu L, Grüner G. A method of printing carbon nanotube thin films. Applied Physics Letters 2006, 88: 1.

[15] Doherty EM, De S, Lyons PE, Shmeliov A, Nirmalraj PN, Scardaci V, Joimel J, Blau WJ, Boland JJ, Coleman JN. The spatial uniformity and electromechanical stability of transparent, conductive films of single walled nanotubes. Carbon 2009, 47: 2466.

[16] Blighe F.M, Lyons PE, De S, Blau WJ, Coleman JN. On the factors controlling the mechanical properties of nanotube films. Carbon 2008, 46: 41.

[17] Blighe FM, Blau WJ, Coleman JN. Towards tough, yet stiff, composites by filling an elastomer with single walled nanotubes at very high loading level. Nanotechnology 2008, 19: 1.

[18] Chen Q, Bao J, Park J, Liang Z, Zhang C, Wang B. High mechanical performance composite conductor: Multi-walled carbon nanotube sheet/bismaleimide nanocomposites. Advanced Functional Materials 2009, 19: 3219.

[19] Guo S, Zhang C, Wang W, Liu T, Chauhari WT, He C, Zhang WD. Preparation and characterization of polyurethane/multiwalled carbon nanotube composites. Polymer & Polymer Composites 2008, 16: 471.

[20] Kim H, Miura Y, Macosko CW. Graphene/polyurethane nanocomposites for improved gas barrier and electrical conductivity. Chemistry of Materials 2010, 22: 3441.

[21] Fernández-d'Arlas B, Rueda L, de la Caba K, Mondragon I, Eceiza A. Microdomain composition and properties differences of biodegradable polyurethanes based on MDI and HDI. Polymer Engineering and Science 2008, 48: 519.

[22] ASTM-D 4274-88. Standard test methods for testing polyurethane raw materials: Determination of hydroxyl numbers of polyols. Test Method A, 2005.

[23] Hu H, Bhowmik P, Zhao B, Hamon MA, Itkis ME, Haddon RC. Determination of acid sites of purified single-walled carbon nanotubes by acid-base titration. Chemical Physics Letters. 2001, 345: 25.

[24] Fernandez d´Arlas B, Goyanes S, Rubiolo GH, Mondragon I, Corcuera M, Eceiza A. Surface modification of multiwalled carbon nanotubes via esterification using a biodegradable polyol. Journal of Nanoscience and Nanotechnology 2009, 9: 6064.

[25] Giordani S, Bergin SD, Nicolosi V, Lebedkin S, Kappes MM, Blau WJ, Coleman JN. Debundling of single-walled nanotubes by dilution: Observation of large populations of individual nanotubes in amide solvent dispersions. Journal of Physical Chemistry B 2006, 110: 15708.

[26] Thostenson ET, Chou TW. On the elastic properties of carbon nanotube-based composites: Modelling and characterization. Journal of Physics D: Applied Physics 2003, 36: 573.

[27] Blighe FM, Hernandez YR, Blau WJ, Coleman JN. Observation of percolation-like scaling-far from the percolation threshold-in high volume fraction, high conductivity polymer-nanotube composite films. Advanced Materials 2007, 19: 4443.

[28] Xia H, Song M. Preparation and characterization of polyurethane-carbon nanotube composites. Soft Matter 2005, 1: 386.

[29] Lv RH, Xu W, Na B, Chen B. Insight into the role of filler network in the viscoelasticity of a carbon black filled thermoplastic elastomer: A strain dependent electrical conductivity study. Journal of Macromolecular Science B: Physics 2008, 47: 774.

[30] Koerner H, Liu W, Alexander M, Mirau M, Dowty H, Vaia RA. Deformation-morphology correlations in electrically conductive carbon nanotube thermoplastic polyurethane nanocomposites. Polymer 2005; 46: 4405.

[31] Fernández-d'Arlas B, Khan U, Rueda L, Coleman J. N, Mondragon I, Corcuera M.A, Eceiza A, Influence of hard segment content and nature on polyurethane/multiwalled carbon nanotube composites, Composites Science and Technology 2011, 71: 1030.

[32] Bowyer WH, Bader MG. On the reinforcement of thermoplastics by imperfectly aligned discontinuous fibres. Journal of Materials Science 1972, 7: 1315.

[33] Krenchel H. Fibre reinforcement. Akademisk Forlag, Copenhagen, 1964.

[34] Yu MF, Lourie O, Dyer MJ, Moloni K, Kelly TF, Ruoff RS. Strength and breaking mechanism of multiwalled carbon nanotubes under tensile load. Science 2000, 287: 637.

[35] Xie S, Li W, Pan Z, Chang B, Sun L. Mechanical and physical properties on carbon nanotube. Journal of Physics and Chemistry of Solids 2000, 61: 1153.

[36] Kelly A, Tyson WR. Tensile properties of fibre-reinforced metals: Copper/tungsten and copper/molybdenum. Journal of Mechanics and Physics of Solids. 1965, 13: 329.

[37] Lee CH, Liu JY, Chen SL, Wang YZ. Miscibility and properties of acid-treated multi-walled carbon nanotubes/polyurethane nanocomposites. Polymer Journal 2007, 39: 138.

[38] Chen W, Tao X, Liu Y. Carbon nanotube-reinforced polyurethane composite fibers. Composites Science and Technology 2006, 66: 3029.

[39] Coleman JN, Khan U, Blau WJ, Gun´ko YK. Small but strong: A review of the mechanical properties of carbon nanotube-polymer composites. Carbon 2006, 44: 1624.

[40] Halpin JC, Kardos JL. The Halpin-Tsai equationss: a review. Polymer Engineering and Science 1976, 16: 344.

[41] Frisch HL, Hammersley JM. Percolation processes and related topics. Journal of the Society for Industrial and Applied Mathematics. 1963, 11: 894.

[42] Guth E. Theory of filler reinforcement. Journal of Applied Physics 1945, 16: 20.

[43] Cox HL. The elasticity and strength of paper and other fibrous materials. British Journal of Applied Physics. 1952, 3: 72.

[44] Liff SM, Kumar M, McKinley GH. High-performance elastomeric nanocomposites via solvent-exchange processing. Nature Materials 2007, 6: 76.

[45] Sahoo NG, Jung YC, Yoo HJ, Cho JW. Effect of functionalized carbon nanotubes on molecular interaction and properties of polyurethane composites. Macromolecular Chemistry and Physics 2006, 207: 1773.

Acknowledgements

Financial support from Spanish *Ministerio de Ciencia e Innovación* (TME-2008-01156) and Basque Country Governments in the frame of CIC-*i*nanoGUNE-ETORTEK 0911, *Grupos Consolidados* (IT-365-07) and SAIOTEK S-PE09UN07 is gratefully acknowledged. The authors also wish to acknowledge SGIker, General Research Services from the University of the Basque Country, for their support with the atomic force (*Macroconducta-Mesoestructura-Nanotecnología* unit) and scanning electron microscopes (*Microscopía Electrónica y Microanális de Materiales* unit).

Figures

Fig. 1. Length distributions of oxidised (A) and pristine nanotubes (B) as obtained by atomic force microscopy**.** Multiwalled carbon nanotube pristine network characterised by C) Atomic force microscopy and D) Scanning electron microscopy with scale bar of 100 nm.

Fig. 2. Representative tensile stress-strain (σ-ε) curves for the indicated systems. In the inset the strain scale is logarithmic.

Fig. 3. Composites properties evolution with nanotubes concentration. (■) Solvent cast composites and (Δ) Infiltrated buckypaper composites tested at 1mm min^{-1}.

Fig. 4. A) Composites strength results against nanotube volume fraction. The dashed line is the linear fit from where the critical length was estimated using Eq. (1) for aligned short fibres ($l < l_c$). B) Elastic modulus of composites. The dotted line is the prediction of Eq. (2) with $\eta_0 = 1/5$ using the l_c previously calculated. The dashed line represents the same model but with $\eta_0 = 1$. c) Low volume fraction region of (B) in non-logarithmic scale. In all cases (■) solvent cast composites; (○) Infiltrated buckypapers tested at 100 mm min^{-1} and (Δ) Infiltrated buckypapers tested at 1 mm min^{-1}.

Fig. 5. A) Fracture surface of a 18 wt% MWCNT infiltrated buckypaper. Scale bar 1 μm. (B,C) 2 μm x 2 μm atomic force microscopy images of a composite with 6 wt% MWCNT before and after testing, respectively. The arrows indicate the stress direction in the fracture process. These samples were strained at 100 mm min^{-1}.

Fig. 6. Dynamic mechanical storage modulus (E') and loss factor (tan δ) of the indicated solvent cast and infiltrated buckypaper (BP) composites.

Fig.7. Evidence of MWCNT-hard segments interactions observed in A) FT-IR spectra of composites with different MWCNT content. In the inset the peaks ratio absorbance h_a/h_f is represented against MWCNT content. B) DSC heating scans of composites with different MWCNT content.

Tables

Table 1. Specific properties of infiltrated buckypapers. Infiltration solutions remarks and final buckypapers composite composition, density and porosity properties (Further information in methods).

mL solution	[PU10] (mg mL^{-1})	[MWCNT] (wt%)	[MWCNT] (ϕ)	ρ (kg m^{-3})	Porosity
0	**0**	100	1	268	0.80
15	**1**	73	0.62	*	*
25	**1**	74	0.64	*	*
50	**1**	73	0.62	362	0.76
100	**1**	69	0.57	516	0.65
50	**2**	18	0.12	948	0.19
50	**10**	6	0.04	1064	0.05

* Not measured

Fig.1

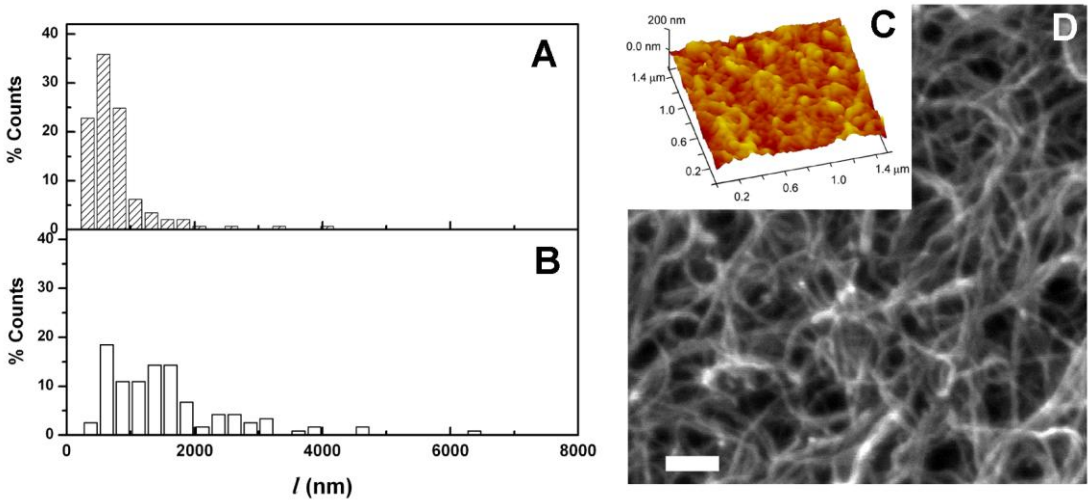
A
B
C
D
% Counts
% Counts
l (nm)
200 nm
0.0 nm
1.4 μm
1.4 μm

Fig.2

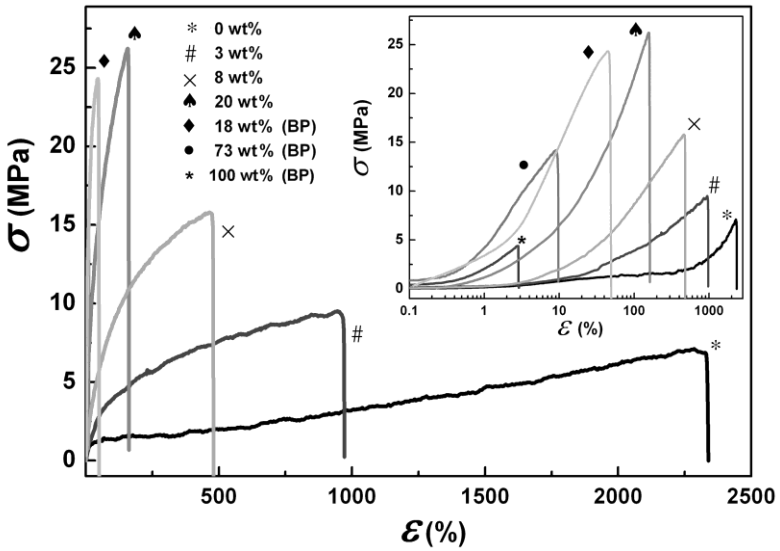
0 wt%
3 wt%
8 wt%
20 wt%
18 wt% (BP)
73 wt% (BP)
100 wt% (BP)
σ (MPa)
ε (%)

Fig.3

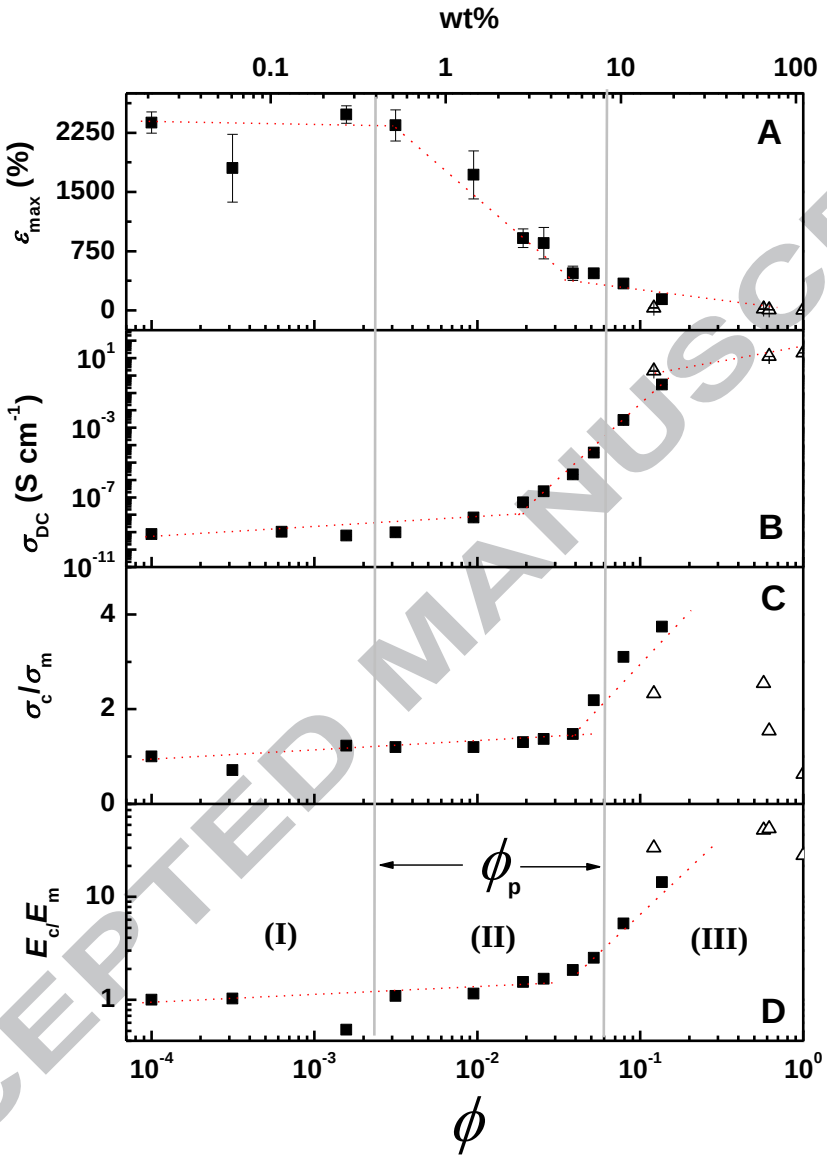

Fig. 4

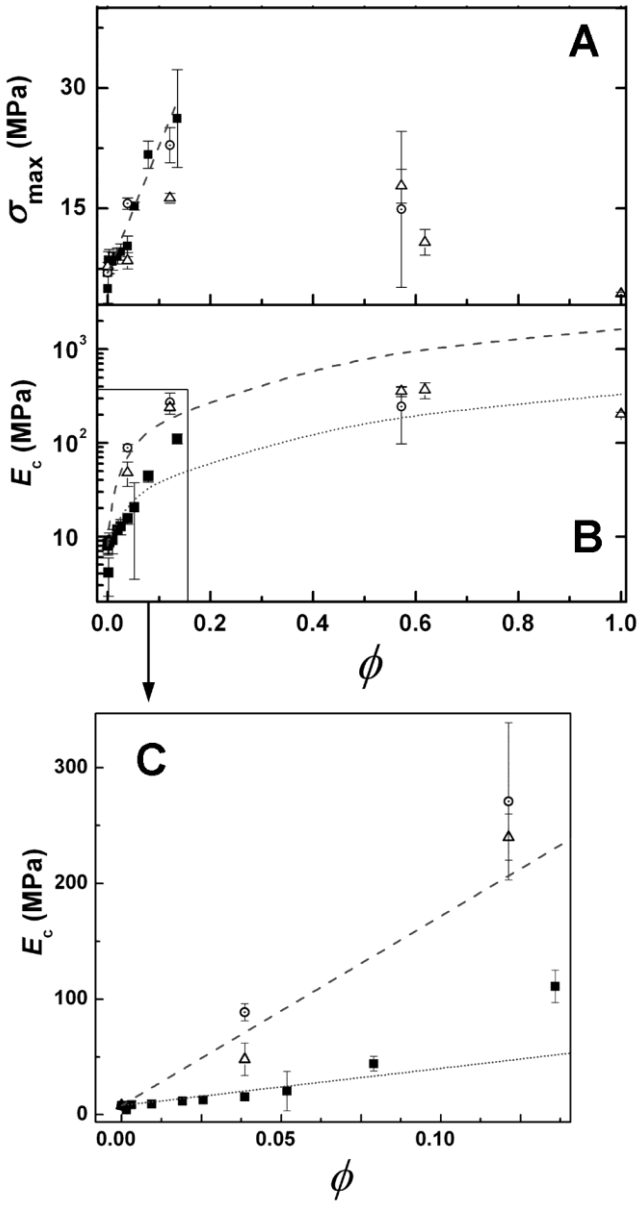

Fig. 5

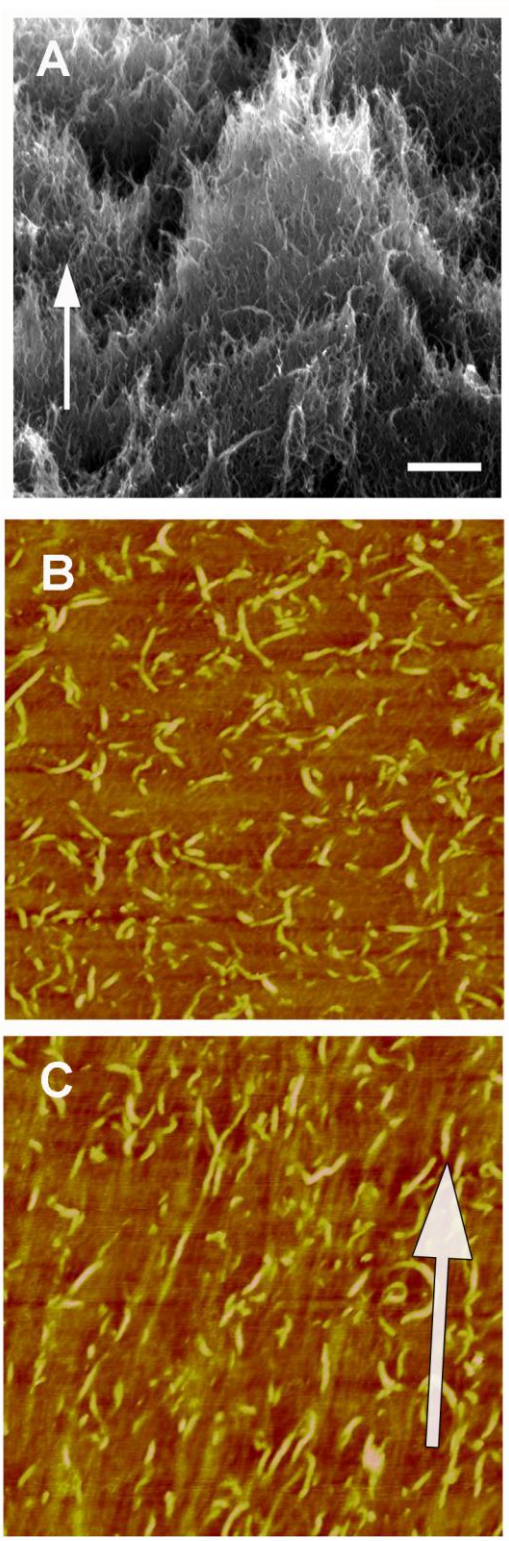

Fig. 6

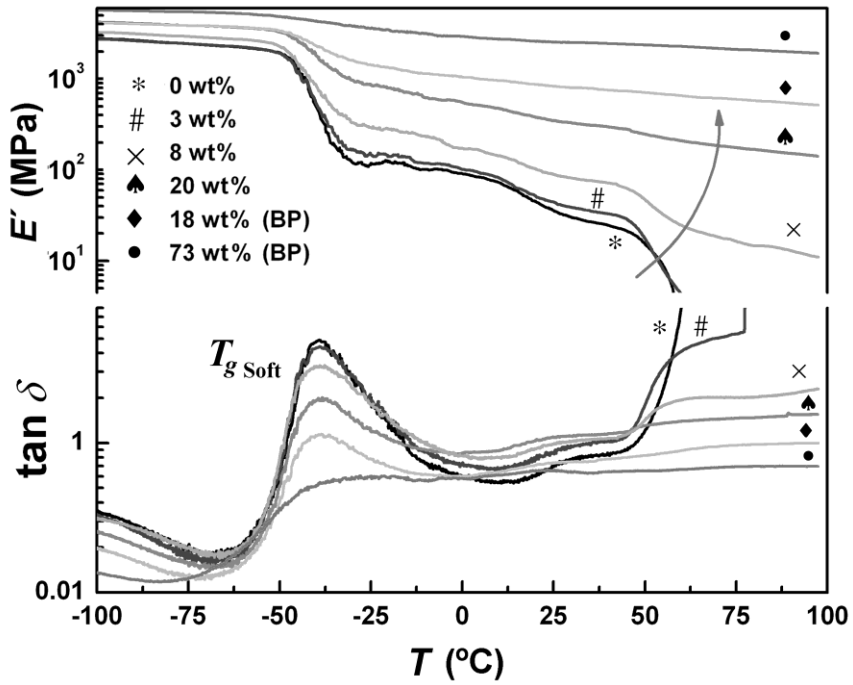

Fig.7

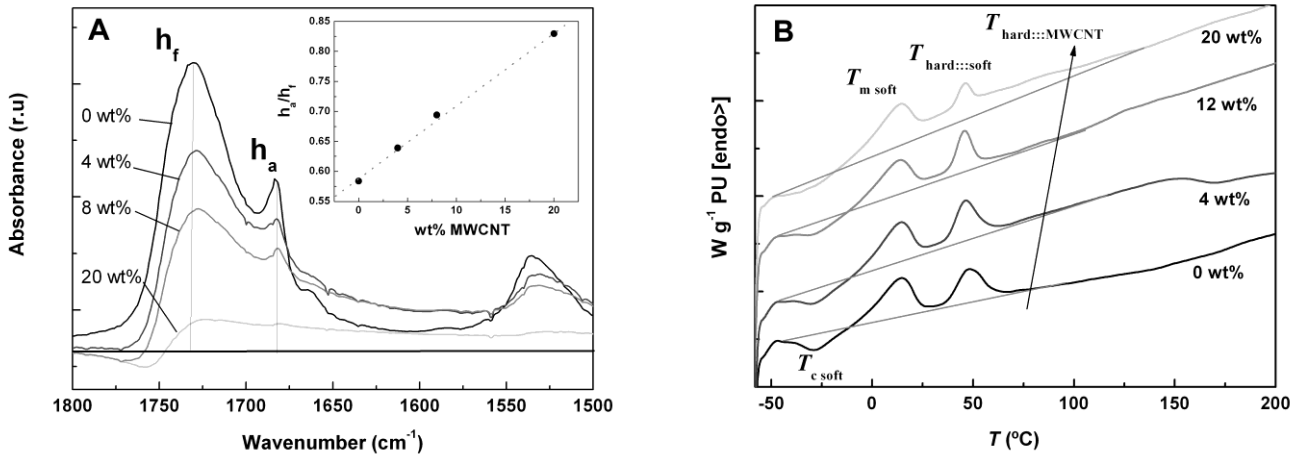

Supplementary

S1

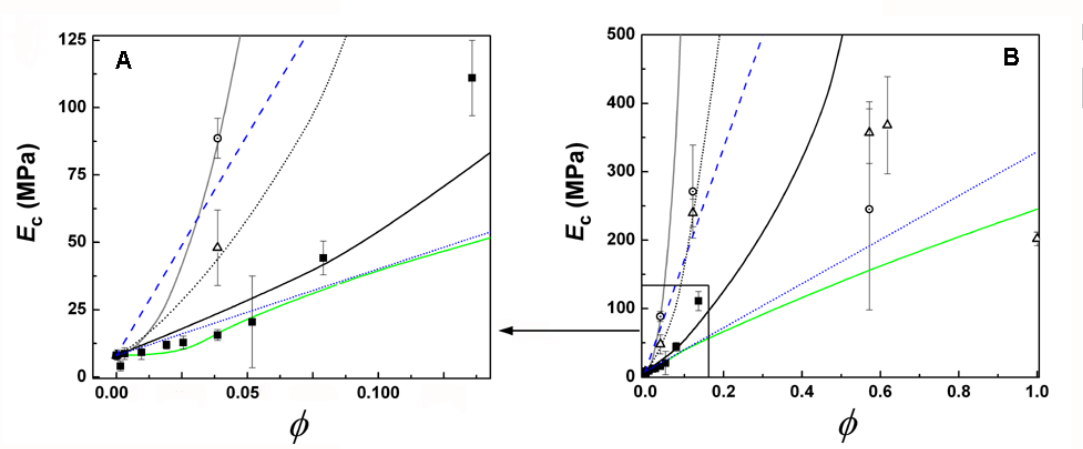

Fig. S1. Typical models for reinforced elastomers. Elastic modulus of composites, E_c, versus multiwalled carbon nanotubes (MWCNT) volume fraction, ϕ. a) A zoomed region for low ϕ of (b). The Guths model (ref. 39) extended for anisotropic fillers, widely employed in elastomers, was considered:

$$E_c = E_m(1 + 0.675(l/D)\phi + 1.62(l/D)^2\phi^2$$

where E_m is the modulus of the neat polyurethane. This model considers that the fibre elastic modulus is orders of magnitude higher than that of the matrix. The utilised (l/D) aspect ratio was obtained experimentally from AFM statistical analysis and was averaged to be l/D = 62. This is represented with a grey line. The model resulted to overestimate both solvent cast an infiltrated buckypapers elastic modulus.

The blue dashed and dotted curves correspond to Bowder-Boyer models already commented in the text, with η_0 = 1 for aligned fibres and η_0 = 1/5 for randomly oriented fibres, respectively.

The black dotted line corresponds to the rule of mixtures as modified by Cox (ref. 40), similar to the Bowder-Boyer model but with a length efficiency factor given by

$\eta_l = 1 - \left[Tanh(a \cdot l/D) / (a \cdot l/D) \right]$ with $a = \sqrt{-3E_m / 2E_f \ln \phi}$.

Another used model was the Halpin-Tsai modified for randomly oriented fibres:

$$E_c = E_m \left[\frac{3}{8} \left(\frac{1 + \zeta \eta_L \phi}{1 - \eta_L \phi} \right) + \frac{5}{8} \left(\frac{1 + 2\eta_T \phi}{1 - \eta_L \phi} \right) \right]$$

where $\zeta = 2l/D$, $\eta_L = (E_f/E_m - 1)/(E_f/E_m + \zeta)$, and $\eta_T = (E_f/E_m - 1)/(E_f/E_m + 2)$.

The Halpin-Tsai model (solid black curve) resulted to slightly overestimate modulus data of composites prepared by the solvent casting approach up to a concentration of nanotubes of about 12 wt% (ϕ = 0.08). Upon that value it underestimated the modulus of higher loadings composites prepared by this approach. The reinforcement predicted by the model for $\phi \to 0$ (ref. 36), $dE_c/d\phi \approx (3/8)E_m \eta_L(\xi + 1) + (15/8)E_m$ = 389 MPa (using E_f = 500 GPa), what is in good agreement with that obtained experimentally (slope of Fig. S1a-b) as calculated with data from 0 wt% to 20 wt% MWCNT (ϕ = 0.13) of $dE_c/d\phi$ = 361 ± 41 MPa.

The last model to consider for modulus prediction was that based of the general theory for percolative systems which allows to predict composite properties above the percolation threshold or filler network formation at critical concentration. Behaviour of the properties of such percolated systems usually follows a power-law scaling:

$$E_c = E_m + A(\phi - \phi_p)^t$$

valid for $\phi > \phi_p$, where ϕ_p is the percolation threshold volume fraction of the MWCNT into the polyurethanes matrix, and A and t are model parameters, which depend on nanofiller shape and dimensions and sample geometry. From the slope of log (E_c) vs.

$\log(\phi - \phi_p)$, with ϕ_p = 0.025, values of A = 240.4 MPa and t = 0.78 were obtained. This model, represented with a green curve in Fig. 3d,e resulted to adjust pretty well the composites modulus up to 12 wt% and underestimated both composites and buckypapers with MWCNT content higher than 18 wt%. Surprisingly this model predicted very well the modulus of the pure MWCNT buckypaper. This could mean that in the reinforcement of a polymer with MWCNT the formation of a jammed network like structure, behaviour predicted by the model, could be of great importance on final elastic properties of the material.

S2

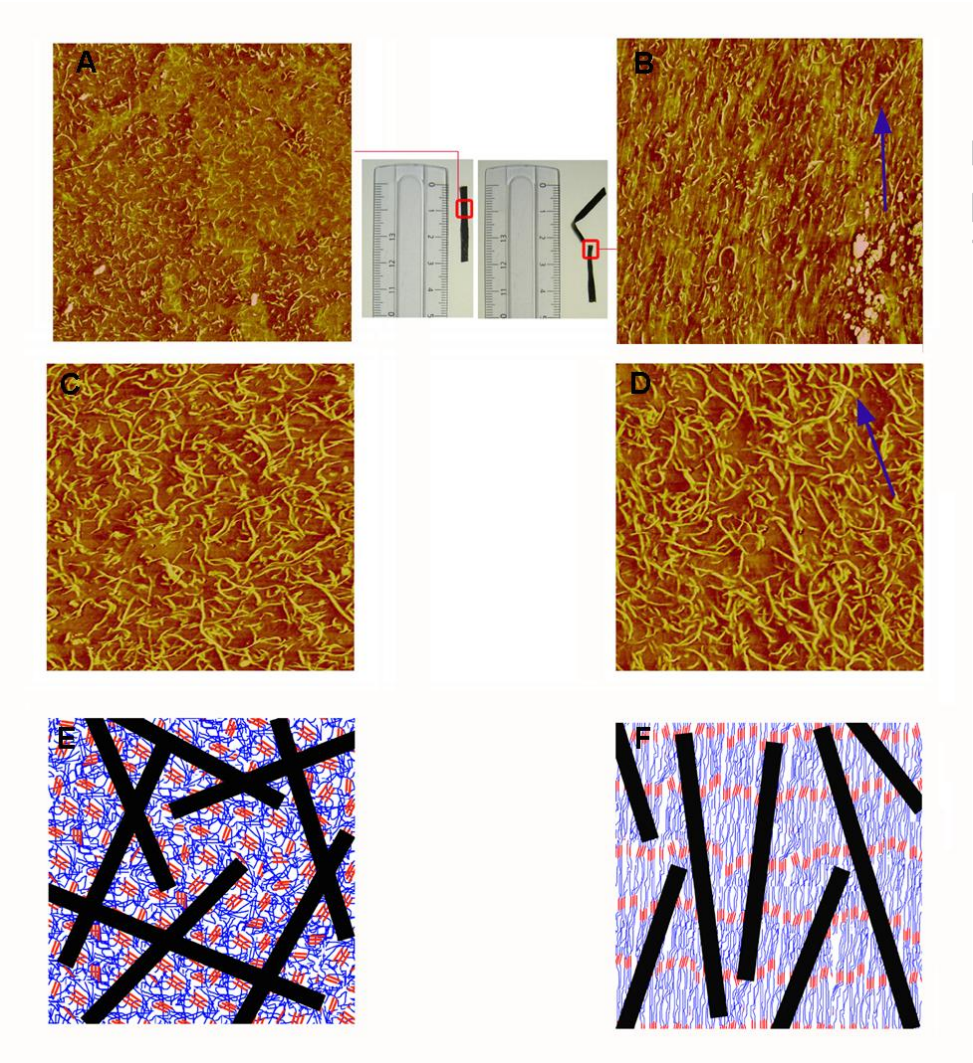

Fig. S2. Multiwalled carbon nanotubes (MWCNT) alignment with stress in an elastomeric polyurethane (PU) matrix, monitored by atomic force microscopy (AFM). 5 μm x 5 μm AFM scans of a 6 wt% solvent cast composite before (a) and after (b) testing with indication of the representative zones of the probes scanned in each case before and after testing. A 2 μm x 2 μm image of a solvent cast composite with 12 wt% MWCNT before (c) and after testing (d). The samples were tested at 100 mm min^{-1} and scanned in the AFM after two months from the tensile tests. In e and f schematic representations of MWCNT and polyurethanes domain rearrangement along stress

direction before and after testing are depicted. These experiments further suggest that MWCNT were preferentially orientated along the stress direction, allowing us to consider a varying orientation factor during stress application, and to successfully apply Eqs (1) and (2) at fracture and initial stages, respectively.